Fragmentation of two soft cereal products during oral processing in the elderly: Impact of product properties and oral health status

Melissa Assad Bustillos, Carole Tournier, Gilles Feron, Sofiane Guessasma, Anne-Laure Reguerre, Guy Della Valle

Fragmentation of two soft cereal products during oral processing in the elderly: impact of product properties and oral health status

Assad-Bustillos, M.[1,2,3], Tournier, C[2]., Feron G[2]., Guessasma[1], S., Reguerre A.L.[1], Della Valle, G[1*].

[1] *INRA UR-1268 Biopolymères Interactions et Assemblages, 44316 Nantes, France*

[2] *Centre des Sciences du Goût et de l'Alimentation, AgroSup Dijon, CNRS, INRA, Université Bourgogne Franche-Comté, F-21000 Dijon, France*

[3] *CERELAB®, La Sucrerie 21110 Aiserey, France*

*corresponding author : guy.della-valle@inra.fr

Abstract

This study investigated the mechanisms of fragmentation leading to bolus formation during chewing in the elderly population for two cereal foods of different compositions and cellular structure: sponge-cake (SC) and brioche (B). For both products, mechanical properties were characterized by uniaxial compression and 3D cellular structure was determined using x-ray micro-tomography. Stress-strain curves showed two distinct ductile-like behaviors: product B underwent plastic deformation, whereas product SC displayed a hyper-elastic behavior. Twenty subjects aged 65 years and over with two different oral health conditions (poor *vs* satisfactory dental status, variable stimulated salivary flow rate) were asked to consume both products. Bolus particle size was determined at three different chewing stages through image analysis, and the resulting particle size distribution (PSD) curves were fitted by Gompertz model. The model parameters were related to bolus particle heterogeneity and fragmentation, thanks to their correlations with median particle size diameter D_{50} and interquartile ratio (D_{75}/D_{25}), directly extracted from PSD curves. The use of model parameters allowed discriminating between chewing sequences for both products and revealed different fragmentation patterns: while SC boli exhibited a continuous particle size reduction during chewing, B displayed a combination of fragmentation and agglomeration. In addition, results showed that subjects with a satisfactory dental status produced significantly more degraded boli than those with a poor dental status. These results highlight distinct fragmentation mechanisms for these two soft

products that were interpreted in relation to their differences in composition, structure and mechanical behavior.

Nomenclature

a	Gompertz fitting parameter, maximum size value achieved
ANSM	Acronym for the French 'National Agency of Drugs and Safety'
B	Brioche
b	Gompertz fitting parameter, slope at the inflexion point
c	Gompertz fitting parameter, size value at the inflexion point
C1	1/3 of chewing duration, first chewing sequence
C2	2/3 of chewing duration, second chewing sequence
D_{25}	Particle diameter of first the quartile of the distribution
D_{50}	Median particle diameter of the distribution
D_{75}	Particle diameter of the third quartile of the distribution
$D_{75/25}$	Interquartile ratio of the particle size distribution
DS	Dental status
E	Young's modulus (kPa)
FOP	Food Oral Processing
P	Poor (Dental status)
PSD	Particle Size Distribution
PFU	Posterior Functional Unit
S	Satisfactory (Dental status)
SC	Sponge-cake
SP	Swallowing Point, total chewing duration, third chewing sequence,
SSF	Stimulated Salivary Flow rate ($mL \cdot min^{-1}$)
XR-µCT	X-Ray Micro-Computed Tomography

σ_c Critical stress (kPa)

1. Introduction

The physiological deterioration that accompanies ageing, together with the fact that the population aged 60 and over is expected to nearly triple by 2050 (United Nations, 2002), have increased the demand for foods with optimum texture design that are nutritious, safe and enjoyable (Chen, 2016; Schwartz, Vandenberghe-Descamps, Sulmont-Rossé, Tournier, & Feron, 2017).

Peleg early pointed out the need for understanding the relationship between the mechanical and geometrical properties of a food and its perceived texture in order to provide guidelines to develop specific products targeted for the elderly (Peleg, 1993). Since then, advances in the understanding of food oral processing (FOP) have been extensively reviewed (Chen, 2009, 2014, 2015) and the importance of structure and mechanical properties of foods in the bolus formation mechanisms has been highlighted (Gao, Wang, Dong, & Zhou, 2017; Pascua, Koç, & Foegeding, 2013; Witt & Stokes, 2015), as well as in the perception of flavor (Panouillé, Saint-Eve, Déléris, Le Bleis, & Souchon, 2014) and texture (Devezeaux de Lavergne, Derks, Ketel, de Wijk, & Stieger, 2015; Gao, Ong, Henry, & Zhou, 2017). These works have improved the understanding of texture by combining the studies of bolus formation mechanisms with the structural and mechanical properties of foods. The perception of texture is recognized as a dynamic process and does not depend only on the initial food properties, which govern the early stages of mastication (Kim et al., 2012; Young, Cheong, Hedderley, Morgenstern, & James, 2013), but also on bolus properties towards the middle and the end of oral processing (Devezeaux de Lavergne, van de Velde, & Stieger, 2017; Jourdren, Saint-Eve, et al., 2016). The

84 characterization of bolus properties has thus become crucial to the understanding of
85 FOP and perception mechanisms. This approach has been poorly addressed in the
86 elderly, despite that such knowledge could bring new opportunities to develop food
87 products specifically targeted for this population. Recently, we studied the
88 relationships between sensory perception, food oral processing and bolus properties
89 for two cereals products, namely sponge-cake and brioche, in elderly subjects
90 varying in dental status and salivary flow rate (Assad-Bustillos, Tournier, Septier,
91 Della Valle, & Feron, 2017). We developed a phenomenological model predicting the
92 evolution of bolus apparent viscosity during oral processing. Viscosity was found to
93 decrease with the theoretical amount of saliva absorbed, expressed as the product of
94 chewing time by the stimulated salivary flow rate, irrespectively of the dental status of
95 the subjects (Assad-Bustillos et al., 2017). However, the model displayed some
96 dispersion, likely because the contribution of the particle size distribution of bolus
97 fragments (PSD) was not taken into account.
98 The PSD of foods during oral processing has been early recognized as a crucial
99 factor in bolus formation (Hoebler, Devaux, Karinthi, Belleville, & Barry, 2000; Olthoff,
100 Van Der Bilt, Bosman, & Kleizen, 1984; Peyron, Mishellany, & Woda, 2004), and has
101 been identified as a key parameter in the triggering of swallowing (Jalabert-Malbos,
102 Mishellany-Dutour, Woda, & Peyron, 2007; Peyron et al., 2011). Many studies have
103 attempted to describe the comminution process of food materials after chewing by
104 using mathematical models that consider the probability of a particle of being
105 selected and its degree of fragmentation, which in turn depend on other factors such
106 as its shape and mechanical properties (Lucas & Luke, 1983; van der Bilt, Olthoff,
107 van der Glas, van der Weelen, & Bosman, 1987; van der Glas, Kim, Mustapa, &
108 Elmanaseer, 2018; van der Glas, van der Bilt, & Bosman, 1992). To this extent, there

109 have been attempts to relate the degree of fragmentation of several foods to their
110 mechanical properties (Agrawal, Lucas, Prinz, & Bruce, 1997; Chen, Khandelwal, Liu,
111 & Funami, 2013; Lucas, Prinz, Agrawal, & Bruce, 2002). From these studies, it
112 appears that the median particle size (D_{50}) of the bolus before swallowing is inversely
113 related to the food hardness obtained from instrumental measurements performed by
114 uniaxial compression. However, these observations seem to be limited to foods that
115 exhibit brittle facture, meaning that they break in their elastic domain. As pointed out
116 by Gao, Wang, et al. (2017), there is a lack of similar studies concerning fracture in
117 ductile (also referred as *soft*) food materials, which are able to resist high levels of
118 plastic deformation before breaking (e.g. bread or cakes).
119 As far as we know, the only cereal food exhibiting ductile behavior for which PSD
120 after chewing has been studied and modelled is bread. Different methods have been
121 used to characterize the PSD, such as drying, sieving and weighing the recovered
122 fractions. Image acquisition - based on optical scanning, camera and/or laser
123 diffraction for small particles (≤ 1mm) (Jourdren, Panouillé, et al., 2016; Le Bleis,
124 Chaunier, Della Valle, Panouillé, & Réguerre, 2013; Pentikäinen et al., 2014) (Gao,
125 Wong, Lim, Henry, & Zhou, 2015; Hoebler et al., 1998, 2000) - have been used to
126 provide a more accurate quantitative analysis. The diversity of methods used has
127 made it difficult to compare results between studies. Yet, all of them concluded that
128 there is a general decrease of the median particle size (D_{50}) over time, and Jourdren,
129 Panouillé, et al., 2016 also reported an increase in bolus heterogeneity, which they
130 chose to assess by the interquartile ratio (D_{75}/D_{25}). In contrast, the influence of the
131 initial bread structure in the PSD has not been extensively studied, and so far the
132 reported results lack of consensus. For instance, Pentikäinen et al. (2014) showed
133 that rye wholegrain breads, which featured denser structures and thicker cell walls

than traditional wheat bread, led to boli that contained smaller particles. Yet, in a similar study, Le Bleis, Chaunier, Montigaud, & Della Valle (2016) found no significant effect of structure in the D_{50} of boli from fiber-rich bread with different densities. In general, inter-individual variability is considered to have a large influence on oral processing and bolus properties (Panouillé, Saint-Eve, & Souchon, 2016). However, when it comes to particle size, the impact of physiology has rarely been taken into account (Fontijn-Tekamp, van der Bilt, Abbink, & Bosman, 2004; Hoebler et al., 1998; Peyron et al., 2004). Furthermore, there is a lack of focus on the elderly population, whose oral health is frequently deteriorated due to tooth loss and decreased salivary flow rate (Laguna, Aktar, Ettelaie, Holmes, & Chen, 2016; Ship, 1999; Vandenberghe-Descamps et al., 2016).

Hence, considering the various aspects involved in food fragmentation and bolus formation, the objectives of this study were, in the first place, to accurately describe and assess the fragmentation process during the chewing of two soft cereal foods with different composition and structure in an elderly panel; and secondly, to assess the impact of the oral health status of the participants in the said foods' fragmentation process. In this purpose, we have fully characterized the PSD of sponge-cake (SC) and brioche (B) boli collected after three chewing stages from a group of elderly subjects. Additionally, the data was fitted with a mathematical model in order to be able to extract as much information as possible and avoid single parameter comparisons. With this information, the influence of the dental status (DS) and salivary flow rate (SSF) of the elderly on the PSD of the boli was evaluated.

2. Materials and Methods

2.1 Product composition, structural and mechanical properties

158 The sponge-cake and brioche used in this study were provided by CERELAB®,
159 France. Their composition is detailed in Table A (Appendix).
160 Their instrumental texture was defined by their density, 3D cellular structure and
161 mechanical behavior. The product density was measured by the rapeseed
162 displacement method.
163 The three-dimensional cellular structure was determined by X-ray micro-computed
164 tomography (XR-µCT), using a compact table-top system Skyscan 1174 (Bruker
165 microCT, Belgium). A cylindrical sample of each product with a diameter of 2 cm and
166 a height of 3 cm was prepared with a steel cutter and placed on a rotating plate while
167 the X-ray beam passed through. A CCD camera with a resolution of 1304×1304
168 pixels was used to acquire the 2D radiographic images. The exposure time was 2000
169 ms, and the pixel size was adjusted to 22 µm. Two images were taken per rotational
170 step (every 0.5°, until 360°) and were averaged. The projections were then
171 reconstructed to obtain cross-sectional images using the NRecon reconstruction
172 software (Bruker microCT, Belgium). Reconstructions were based on the Feldkamp
173 cone-beam algorithm (Feldkamp, Davis, & Kress, 1984). After reconstruction, a stack
174 of 1000 images in TIFF format was obtained for each sample. 3D images were
175 therefore composed of 1304×1304×1000 voxels, coded on an 8-bit grey-scale. One
176 replication was made for each product, for a total of four independent 3D images
177 generated. From the images, the granulometric curves, that lead to cell wall size and
178 cell wall thickness values, were calculated by using mathematical morphology
179 operations (Serra, 1982). A series of openings of increasing size (image sieving)
180 was performed on the features of interest and the sum of the volume occupied by the
181 sieved particles, either cells or walls, was computed at each step. The results were
182 expressed as the plot of the cumulative volume (%) of the particle *vs* the particle

183 diameter (µm). In addition, the relative density (D) was calculated by dividing the
184 volume occupied by the cell walls by the total volume of the sample, and the void
185 fraction (VF), or porosity (P), was calculated as the complementary fraction D (1)

186 $$P = VF = 1 - D \qquad (1)$$

187 The mechanical properties were determined by uniaxial compression test. A circular
188 steel cutter was used to prepare cylindrical samples with a diameter of 40 mm and a
189 height of 30 mm. Both products were subjected to uniaxial compression using a
190 universal testing machine (Adamel Lomarghy, France) equipped with a 1 kN load
191 cell. The testing was performed with a cross head speed of 50 mm/min until 66% in
192 height reduction between parallel plates. Five replicates were performed for each
193 food sample. Results were expressed as the stress versus strain plot, from which
194 Young's modulus (E), and the critical stress (σ_c), when applicable, were measured. E
195 was calculated from the initial slope within the linear elastic domain, while σ_c was
196 defined as the stress value at the end of the linear domain.

197 *2.2 Panel composition*

198 Twenty subjects (9 men and 11 women, aged 65–82 years, average 72 ± 5 years)
199 participated in the study. Their dental status (DS) was assessed by determining the
200 number of Posterior Functional Units (PFU's), allowing their classification within two
201 groups: poor (≤ 4PFU's) and satisfactory (≥7 PFU's) DS. Additionally, their salivary
202 flow rate in $mL \cdot min^{-1}$ under mechanical stimulation (SSF), was determined for each
203 subject. The chewing duration up to the swallowing point (SP) was determined for
204 each subject and product through video recording. These techniques were previously
205 used and detailed by Assad-Bustillos et al. (2017). The results obtained for the
206 average SSF and the SP of all participants, including their standard deviation, are
207 recalled in Table B (See Appendix). All subjects agreed on the content of the study

and signed informed consent. This study was approved by the local ethical committee (CPP Est-I) and the French National Agency of Drugs and Safety (ANSM) (ID RCB n°2016-A00916-45).

2.3 FOP assessment and bolus collection

Mouthfuls of 20 cm^3 of each product were cut right before the experimentation. Each member of the panel was asked to eat a mouthful and to expectorate the generated bolus at three different chewing sequences that were defined according to each individual's swallowing point, as described in detail by Assad-Bustillos et al. (2017). The chewing stages were defined as follows: 1/3 of the total chewing duration (C1), 2/3 of total chewing duration (C2) and just before the swallowing point (SP, total chewing duration). At each chewing sequence, one bolus was generated. The bolus was suspended immediately after collection in 150 mL of glycerol (VWR International, USA) inside a plastic container with a resealable screw-lid and was agitated at room temperature for 1h using a magnetic stirrer at 170 rpm to allow particle dispersion without damaging bolus structure, according to the procedure set up by Le Bleis et al. (2013). The boli were stored at 4°C until the moment of analysis.

2.4 Bolus particle size analysis

Before analysis, the boli suspended in glycerol were re-agitated at a rotation speed of 170 rpm during 80 min at 20°C in a water bath (Julabo SW23, Germany) to ensure homogenous particle dispersion for all samples. Bolus particles were carefully placed in a Petri dish (diameter=5.5 cm) that was placed over a matte dark background and was backlighted through an optical fiber ring (Schott DCR IV, USA) placed underneath, as described by Le Bleis et al. (2013). The images were acquired in gray level with a monochrome CMOS video camera (EXO SVS-250MGE Vistek, Germany). For each bolus, at least 90% of the total volume was characterized, with a

minimum of 10 images per bolus, for a total of 1200 images. Images were saved in TIFF format as matrices of 2448×2048 pixels, with a pixel size of 15 µm. Image analysis was performed with Matlab software (Mathworks 2016b, USA). Particle size distribution (PSD) was obtained using operations of mathematical morphology by performing a series of openings of increasing size (image sieving) as described above for the 3D images. The results were expressed as a plot of the cumulative area (%) of the particle vs the particle diameter in mm, also named PSD curve.

2.5 Data treatment and Statistical analysis

For each subject and each chewing sequence (C1, C2, SP), the median equivalent diameter (D_{50}) and the interquartile ratio (D_{75}/D_{25}) were derived from the PSD curve. The ratio (D_{75}/D_{25}) characterizes the heterogeneity of the bolus (Jourdren, Panouillé, et al., 2016). Moreover, to ascertain their description, all PSD (n=120) were fitted with a three-parameter Gompertz model (2). Gompertz model has been previously used to model the PSD of soils (Botula, Cornelis, Baert, Mafuka, & Van Ranst, 2013; Esmaeelnejad, Siavashi, Seyedmohammadi, & Shabanpour, 2016), *in vitro* degradability of rumen from cereal meals (Gallo, Giuberti, & Masoero, 2016) and to model the porosity kinetics of bread dough during proofing (Kansou et al., 2013). In this study, it is used to model the PSD of food particles after chewing:

$$A = a \times \exp(-\exp(-b \times (p - c))) \qquad (2)$$

Where A is the fraction of cumulated particles area (% of total particle area), p is the particle size (mm), “a”, “b” and “c” are parameters obtained by fitting. Parameter “a” is an approximation of the maximum cumulated area, “b” is the slope of the size distribution curve at the inflection point, and parameter “c” is the particle size at the inflection point. Curve fittings were performed using the modules “NumPy” and “SciPy” from Python v.3.2.5.1 software (Python Software Foundation).

A one-way ANOVA was performed to determine the differences of structural and mechanical properties between the two products. In order to investigate differences between products at each chewing stage, a repeated measures ANOVA (product + subject + chewing sequence) was carried out for the median particle size D_{50}, interquartile ratio D_{75}/D_{25} and Gompertz parameters ("a", "b", "c,"), with the chewing sequence as repeated factor. Additionally, a one-way ANOVA was carried out for each product to investigate differences between chewing sequences. Furthermore, to investigate the impact of oral health status, a three-way ANCOVA (Analysis of covariance) model with level 2 interactions was applied for each product (chewing duration + dental status + stimulated salivary flow + dental status×stimulated salivary flow + dental status×chewing duration + stimulated salivary flow×chewing duration). For every statistical procedure, a significance level of $\alpha=0.05$ was used and results reported according to Type III sum of squares. The Student-Newman-Keuls test was used for post-hoc comparison tests. All statistical analyses were performed with XLSTAT software (v.2016 18.06, Addinsoft, USA).

3. Results and discussion

3.1 Structure and mechanical properties of the two cereal foods

The values of structural and mechanical properties of both products are reported in Table 3, together with their standard deviation. Not surprisingly, both foods show distinct structural features due to their different composition and process. The first indicator of these differences is density, where sponge-cake (SC) showed a lower value ($\rho^*= 0.21$ g.cm^{-3}) than brioche (B) ($\rho^*= 0.33$ g.cm^{-3}). This may be the reason why the cellular structure of SC displayed larger bubbles, or gas cells, while B displayed smaller cells (Fig.1 a, b). From 3D image analysis, the relative density (D)

283 values (D= 0.21 for SC and 0.31 for B) agree with those determined using the
284 rapeseed displacement method (Table 1).
285 From the granulometric curves (Fig.1 c), it can be seen that cell wall size distributions
286 of both foods are close to each other with a median size (D_{50}) value of ≈100 µm and
287 ≈120 µm for SC and B, respectively (Table 1). Regarding the voxel size, i.e. 22 µm,
288 these two values can be considered not significantly different. Conversely, the cells
289 were found significantly larger for SC than B, with a median size of ≈300 µm and
290 ≈200 µm respectively (Table 1). Hence, in line with the difference of density, the main
291 difference in cellular structure between products comes from the cell size.
292 Differences between products with regards to their mechanical behavior can also be
293 observed from the stress-strain curves obtained by compression tests (Fig.2). B
294 behaves like an elasto-plastic material, i.e. that displays inelastic permanent
295 deformation after unloading. Its behavior features a linear elastic part, followed by a
296 plateau-like stage where stress is kept constant due to cell wall buckling and yielding,
297 then followed by a continuous increase of stress reflecting material densification.
298 Conversely, SC behaves like a hyper-elastic material, i.e. it deforms elastically over a
299 large range of loading levels, and its behavior is marked by a continuous increase of
300 the stress until densification. The former behavior has been widely reported in baked
301 products including different types of bread and sponge-cake (Attenburrow,
302 Goodband, Taylor, & Lillford, 1989; Hibberd & Parker, 1985; Scanlon & Zghal, 2001;
303 Wang, Austin, & Bell, 2011). Contrarily, the latter has been rarely observed in starch
304 based food materials (Guessasma & Nouri, 2015; Mohammed, Tarleton,
305 Charalambides, & Williams, 2013). Both behaviors may be assigned to ductile foams,
306 i.e. products that have a large porosity and a cellular structure with cell wall material
307 in the rubbery state, as described by Gibson & Ashby (1997).

The values of Young's moduli (E), for both products, and critical stress (σ_c) for B are reported in Table 1. B had a higher value of E (20 kPa) than SC (5 kPa). This difference may be attributed mainly to the density differences, in line with Gibson & Ashby's (1997) scaling law for solid foams.

Finally, these values of structural and mechanical properties are in the range of those found for other baked products like breads (Besbes, Jury, Monteau, & Le Bail, 2013; Gao et al., 2015; Pentikäinen et al., 2014; Van Dyck et al., 2014) and cakes (Bousquières, Michon, & Bonazzi, 2017; Dewaest et al., 2017; Lassoued, Babin, Della Valle, Devaux, & Réguerre, 2007; Sozer, Dogan, & Kokini, 2011). Median cell size (D_{50}), however, was on the lower edge of the interval [300, 1600µm] encountered in these studies. This could be explained by the high levels of fat of both products, which, according to Brooker (1996), lead to finer crumb grains.

3.2 Particle size distribution (PSD) of the cereal food boli: analysis and curve fitting

Cumulative particle size distributions of food boli (PSD) were determined by quantitative image analysis for each subject, each chewing sequence and each product (Fig. 3). The average values for all subjects of the median diameter (D_{50}) and the interquartile ratio (D_{75}/D_{25}), an indicator of bolus heterogeneity (Jourdren, Panouillé, et al., 2016), were extracted from the PSD curves and are shown in Table 2 for both products. Firstly, B boli had significantly higher D_{50} values than SC at all chewing stages. Secondly, for SC, D_{50} was significantly reduced over the chewing sequences. B boli, on the other hand, did not show any significant variation of D_{50} throughout the chewing stages. Also, D_{50} of B boli showed a higher inter-individual variability than SC, as reflected by the higher standard deviation. In addition, D_{75}/D_{25}, decreased significantly for SC, meaning these boli tend to reduce particle size

towards the same value as mastication progresses. Conversely, this value increased significantly for B boli, meaning particle heterogeneity becomes higher over the chewing sequences. The variations over time of D_{50} and D_{75}/D_{25} for all subjects and both products are shown in Fig. 4. This figure confirms the previous analysis and clearly depicts the scattered variations of D_{50} for B and illustrates the complexity of chewing mechanisms in this product, likely combining fragmentation and agglomeration of food particles.

These results also show that using a single parameter from the PSD, such as D_{50}, is not always sufficient to understand the complex variations of particle size during mastication. Therefore, PSD curves were fitted with the Gompertz three-parameter model described in 2.5 (Fig.3), in order to integrate the whole information brought by these curves and determine if D_{50} and D_{75}/D_{25} conveniently describe those. The average values of the fitting parameters obtained for both products and each chewing sequence are shown in Table 2. Out of 120 fitted PSD curves, 112 of them had a satisfactory fitting ($R^2 \geq 0.9$), 2 had a low quality fitting ($0.6 \geq R^2 \geq 0.8$), and 6 had an unsuccessful fitting ($R^2 \leq 0.5$) (cf. Appendix).

As expected from cumulative curves (Fig.3), “a” coefficient values remain unchanged, close to 100 for all products and chewing sequences, suggesting that the 112 PSD curves of food boli can be described by only the two coefficients “b” and “c”, whose values differ significantly between products for almost every chewing sequence. Coefficient “b” varies significantly between chewing sequences for SC, and coefficient “c” does it for both products. Furthermore, it was found that “c” is positively correlated to D_{50}, (R_{SC}=0.94, R_B=0.95 $p < 0.0001$), and the regression line is closed to the bisector. Conversely, “b” is negatively correlated to D_{75}/D_{25}, (R_{SC}=-0.65, R_B=-0.49 $p < 0.0001$) (Fig. 5). The correlation is particularly satisfactory for both factors in

358 the case of SC. These results confirm that the two coefficients describe completely
359 the variations of particle size boli during chewing. Furthermore, they suggest that the
360 variations of “c” reflect the mean size of bolus particles, and hence their degradation
361 degree: the smaller the “c” value, the more degraded the bolus. Conversely, “b” can
362 be considered as an index of homogeneity of the particle size distribution, at least for
363 SC. These two parameters of the PSD model will be used in the following section to
364 analyze the effect of the oral health status on bolus fragmentation.
365 The remaining 8 “misfit” PSD curves came from boli that featured a high percentage
366 of large size particles, which introduced jaggedness to the distributions, hence
367 making them difficult to fit (see Fig. 3 c,d). Interestingly, all of these boli came from B
368 and belonged to either the second chewing sequence (C2) or the swallowing point
369 (SP). This means the large particles were present by the end of mastication,
370 therefore suggesting agglomeration. Indeed, a closer examination of the PSD curves
371 and bolus images revealed the presence of three fragmentation patterns (cases I, II
372 and III). Case I consists of an overall decrease of particle size over the chewing
373 sequences and an increase in the number of small particles. It is represented by a
374 curve translation towards smaller sizes (Fig 3 a,b). All of the sponge-cake (SC) boli
375 followed case I pattern, with more than 90% of overall particles with a size lower than
376 6 mm (Fig. 6a). This trend was followed for brioche (B) boli for 10 out of 20
377 individuals (Fig. 6b). Out of the remaining 10, 2 showed a clear pattern of
378 agglomeration (case II), which is represented by a translation of the curve towards
379 larger size is with a jagged appearance due to large size particles (>14mm) (Fig. 3c),
380 and is depicted by an increase in particle size during chewing until bolus becomes a
381 single paste-like particle (size ≈20mm) (Fig. 6c). For 8 cases, a non-monotonous
382 variation was found, with two possibilities: either an increment in particle size during

C2 followed by an immediate decrease of particle size at the SP (Fig. 6d), or a decrease in particle size in C2, followed by an increase of particle size in SP (not shown), suggesting a pattern combining agglomeration and fragmentation (case III). Actually, there was no particular relationship between the individual physiology and the agglomeration patterns, for these 10 specific cases as illustrated by Table D (Appendix).

3.3 *Influence of oral health status on bolus fragmentation / agglomeration patterns*

The influence of the oral health status on particle size distributions and model parameters was investigated through ANCOVA model and the results are shown in the present section. In spite of large variations of SSF, from 0.3 to 3.84 mL/min overall (see Table B in Appendix), no significant effect of salivary flow rate (SSF) on D_{50} or PSD model parameters was found for any of the products. For sponge-cake (SC), a significant relationship between dental status (DS) and median particle diameter (D_{50}) was identified ($p<0.05$). The normalized coefficient of the model for the satisfactory DS group (βs) was -0.8. This result means that individuals with a satisfactory DS produced boli with lower D_{50} values than those with a poor DS. The same result was obtained when performing the analysis with “c” Gompertz coefficient instead of D_{50} ($p<0.001$, βs =-1.0). However, in this model, a significant interaction between chewing duration and DS was found ($p<0.01$), where βs =0.6. This positive value may reflect the limited size reduction ($D_{50}\geq 0.15$mm), illustrated in Fig.4a, for longer chewing duration and satisfactory DS. Conversely, for brioche (B), no significant effect of DS was found for D_{50}. A different result was obtained, nonetheless, with “c”, where DS had a significant effect ($p \leq 0.01$, βs =-0.3), meaning this parameter is lower for subjects with a satisfactory DS. This also means that,

contrary to D_{50}, “c” coefficient allows differentiating B boli based on the DS of subjects, and it confirms that Gompertz model parameters more completely account for PSD variations than directly extracted characteristics such as D_{50}. Neither D_{75}/D_{25} nor “b” showed significant relationships with DS or SSF, suggesting that, in the case of these soft cereal foods, bolus particle heterogeneity is independent of the oral health status. Moreover, no particular trend was found with regards to the number of agglomeration cases (n=10) and their distribution according to DS or SSF. More importantly, since no relationship with SSF was found for any of the studied parameters, it is clear that fragmentation does not depend on salivary flow.

3.4 Overall discussion

Our results demonstrate that the Gompertz model accounts for the variability the particle size distribution (PSD) of food particles, and that the two parameters, “b” and “c” that result from it, are sufficient to discriminate between products and chewing sequences. Therefore, they are worth to be related to bolus and chewing characteristics. Also, the analysis of the quality of fit resulted in a quick way to detect atypical data, allowing the identification of different fragmentation patterns in the two studied foods, as discussed in section 3.2. While Sponge-cake (SC) boli featured a monotonous and continuous fragmentation pattern (case I), Brioche (B) boli displayed three different fragmentation patterns (cases I, II and III), including agglomeration in 50% of cases. Moreover, as observed in our previous study (Assad-Bustillos et al., 2017), B boli were perceived as sticky and pasty, which is in agreement with the observed agglomeration patterns observed in the present work. Case I type of behavior has already been observed in other ductile cereal products, like bread (Jourdren, Panouillé, et al., 2016; Le Bleis et al., 2016). However, patterns combining fragmentation and agglomeration during bolus formation, such as cases II

433 and III, have only been reported for brittle cereal products (Rodrigues, Young, James,
434 & Morgenstern, 2014; Young et al., 2013; Yven, Guessasma, Chaunier, Della Valle,
435 & Salles, 2010). Yven et al. (2010) suggested that the transition from fragmentation
436 to agglomeration during chewing is linked to a transition of the material from brittle to
437 ductile. Such shift also seems to depend on the initial structural and mechanical
438 properties of the food, as it occurred faster and was more abrupt for the densest and
439 hardest foods (Young et al., 2013; Yven et al., 2010). Therefore, agglomerative
440 patterns are somehow associated to ductile behavior, and in our case, the structural
441 and mechanical differences between the studied foods are probably responsible for
442 the observed fragmentation mechanisms. Among the two products, B featured a
443 denser structure and higher values for mechanical properties; it also displayed an
444 elasto-plastic behavior, which is known for its low energy dissipation. This means the
445 material can undergo high levels of strain with a relatively small increase in stress. As
446 a result, more energy and effort are needed to break down this type of materials, as
447 much as shearing to allow cell wall breakage. A higher masticatory effort could
448 translate in a longer chewing duration, but also in a bolus formed of larger particles
449 (Gao, Tay, Koh, & Zhou, 2018). In our case, the chewing duration of the two products
450 was similar, yet, the combined effect of a denser structure and elasto-plastic nature
451 could partially account for the higher bolus particle size and agglomerative behavior
452 of B.
453 Conversely, the mechanical behavior of SC was best described by a hyper-elastic
454 constitutive law. Like previously mentioned, this behavior is characterized by a
455 continuous non-linear increase of stress that results from reversible structural
456 modification during compressive loading. However, SC cannot be considered as a
457 true hyper-elastic material since it is neither isotropic nor incompressible (Mihai &

458 Goriely, 2015). From a microstructural point of view, this behavior can be explained
459 by the rearrangement of cells and their modification when loading is applied. In SC, it
460 is clear that failure mechanisms are dominated by irreversible non-plastic
461 deformation. Further experiments using high-resolution 3D image acquisition under
462 compression and shearing would be useful to better understand these mechanisms.
463 Still, it is possible to state that the generated cell wall damage of SC is higher than B
464 at the early stages of compression, thus leading to an increase of stress at a faster
465 rate. This hypothesis would explain why SC was broken down into smaller particles
466 without increasing the chewing duration. Therefore, at product level, differences in
467 fragmentation patterns can be partially explained by the mechanical behavior of the
468 two foods.
469 At the individual level, part of the variability observed in the bolus particle size was
470 explained by the physiology and particularly the dental status (DS) of the elderly
471 subjects. As discussed in section 3.3, a significant relationship between a satisfactory
472 DS and a lower bolus particle size was evidenced for both products. It was also seen
473 that in spite of large variations of stimulated salivary flow rate (SSF), this variable is
474 not involved in the fragmentation process, unlike other bolus properties like hydration
475 or viscosity (Assad-Bustillos et al., 2017). Additionally, no correlation between
476 agglomeration and DS or SSF was found. Still, it is likely that other physiology
477 variables are involved in this mechanism, since agglomeration only occurred in 50%
478 of the cases. According to Prinz & Lucas (1997), the tongue is highly involved in the
479 packing and pressing of bolus particles against the palate. In the elderly, the tongue
480 and cheek muscles that are associated with this function may be altered inducing
481 changes in tongue activity and bite force (Laguna, Sarkar, & Chen, 2015; Laguna et
482 al., 2016; Laguna, Sarkar, Artigas, & Chen, 2015; Peyron, Woda, Bourdiol, &

Hennequin, 2017). Hence, physiological variables such as tongue pressure, tongue muscular activity and bite force may are worth to be taken into account in future studies in order to better understand these mechanisms in the elderly.

Finally, from the ANCOVA analysis performed with Gompertz model parameters, we found that DS has a significant impact on fragmentation. This result suggests that Gompertz parameters provide more information about the fragmentation properties of the food bolus than the parameters extracted directly from the distribution curves. Moreover, modelling the PSD should facilitate the implementation of numerical models based on discrete elements in similar conditions to chewing, like the one proposed by Hedjazi, Martin, Guessasma, Della Valle, & Dendievel (2014).

Conclusion

By using quantitative image analysis of food boli taken at different steps of oral processing, we demonstrated that particle size distribution could be usefully fitted by Gompertz model. This model allows interpreting the food particle size evolution the chewing process in terms of bolus particle heterogeneity and fragmentation. We identified and described different fragmentation mechanisms for two soft cereal products differing in their initial structure and mechanical properties during oral processing in the elderly: sponge-cake was regularly fragmented, whereas brioche agglomerated. These mechanisms were explained the compressive mechanical behavior and intrinsic cell wall properties of the food products. Finally, we put into evidence the importance of the elderly dental status in the fragmentation of both foods, while salivary flow rate was not found to be involved in this process. This study also highlights the need to understand the chewing process of cereal products as a combination of fragmentation and agglomeration mechanisms, and spurs the use of

mathematical models to describe the evolution of particle size in order to be able to take this complexity into account.

Acknowledgements

This work was funded and supported by AlimaSSenS project (ANR- 14-CE20-0003). The authors thank Sylvie Chevallier from ONIRIS Nantes for her assistance in 3D image acquisition and analysis.

References

Agrawal, K. R., Lucas, P. W., Prinz, J. F., & Bruce, I. C. (1997). Mechanical properties of foods responsible for resisting food breakdown in the human mouth. *Archives of Oral Biology*, *42*(1), 1–9.

Assad-Bustillos, M., Tournier, C., Septier, C., Della Valle, G., & Feron, G. (2017). Relationships of oral comfort perception and bolus properties in the elderly with salivary flow rate and oral health status for two soft cereal foods. *Food Research International*, (September), 0–1.

Attenburrow, G. E., Goodband, R. M., Taylor, L. J., & Lillford, P. J. (1989). Structure, mechanics and texture of a food sponge. *Journal of Cereal Science*, *9*(1), IN1-70.

Besbes, E., Jury, V., Monteau, J. Y., & Le Bail, A. (2013). Characterizing the cellular structure of bread crumb and crust as affected by heating rate using X-ray microtomography. *Journal of Food Engineering*, *115*(3), 415–423.

Botula, Y.-D., Cornelis, W. M., Baert, G., Mafuka, P., & Van Ranst, E. (2013). Particle size distribution models for soils of the humid tropics. *Journal of Soils and Sediments*, *13*(4), 686–698.

532 Bousquières, J., Michon, C., & Bonazzi, C. (2017). Functional properties of cellulose
533 derivatives to tailor a model sponge cake using rheology and cellular structure
534 analysis. *Food Hydrocolloids*, *70*, 304–312.
535 Brooker, B. E. (1996). The role of fat in the stabilisation of gas cells in bread dough.
536 *Journal of Cereal Science*, *24*(3), 187–198.
537 Chen, J. (2009). Food oral processing-A review. *Food Hydrocolloids*, *23*(1), 1–25.
538 Chen, J. (2014). Food oral processing: Some important underpinning principles of
539 eating and sensory perception. *Food Structure*, *1*(2), 91–105.
540 Chen, J. (2015). Food oral processing: Mechanisms and implications of food oral
541 destruction. *Trends in Food Science & Technology*, *45*(2), 222–228.
542 Chen, J. (2016). Food for Elderly: Challenges and Opportunities. *Journal of Texture*
543 *Studies*, *47*(4), 255–256.
544 Chen, J., Khandelwal, N., Liu, Z., & Funami, T. (2013). Influences of food hardness
545 on the particle size distribution of food boluses. *Archives of Oral Biology*, *58*(3),
546 293–298.
547 Devezeaux de Lavergne, M., Derks, J. A. M., Ketel, E. C., de Wijk, R. A., & Stieger,
548 M. (2015). Eating behaviour explains differences between individuals in dynamic
549 texture perception of sausages. *Food Quality and Preference*, *41*, 189–200.
550 Devezeaux de Lavergne, M., van de Velde, F., & Stieger, M. (2017). Bolus matters:
551 the influence of food oral breakdown on dynamic texture perception. *Food*
552 *Funct.*, *8*(2), 464–480.
553 Dewaest, M., Villemejane, C., Berland, S., Clément, J., Aliette, V., & Michon, C.
554 (2017). Effect of crumb cellular structure characterized by image analysis on
555 cake softness r o, (October), 1–11.
556 Esmaeelnejad, L., Siavashi, F., Seyedmohammadi, J., & Shabanpour, M. (2016). The

557 best mathematical models describing particle size distribution of soils. *Modeling*
558 *Earth Systems and Environment*, *2*(4), 166.
559 Feldkamp, L. A., Davis, L. C., & Kress, J. W. (1984). Practical cone-beam algorithm.
560 *J. Opt. Soc. Am. A*, *1*(6), 612–619.
561 Fontijn-Tekamp, F. A., van der Bilt, A., Abbink, J. H., & Bosman, F. (2004).
562 Swallowing threshold and masticatory performance in dentate adults. *Physiology*
563 *& Behavior*, *83*(3), 431–436.
564 Gallo, A., Giuberti, G., & Masoero, F. (2016). Gas production and starch degradability
565 of corn and barley meals differing in mean particle size. *Journal of Dairy*
566 *Science*, *99*(6), 4347–4359.
567 Gao, J., Ong, J. J. X., Henry, J., & Zhou, W. (2017). Physical breakdown of bread
568 and its impact on texture perception: A dynamic perspective. *Food Quality and*
569 *Preference*, *60*(May 2016), 96–104.
570 Gao, J., Tay, S. L., Koh, A. H.-S. S., & Zhou, W. (2018). Dough and bread making
571 from high- and low-protein flours by vacuum mixing: Part 3. Oral processing of
572 bread. *Journal of Cereal Science*, *79*, 408–417.
573 Gao, J., Wang, Y., Dong, Z., & Zhou, W. (2017). Structural and mechanical
574 characteristics of bread and their impact on oral processing: a review.
575 *International Journal of Food Science & Technology*, 1–15.
576 Gao, J., Wong, J. X., Lim, J. C.-S., Henry, J., & Zhou, W. (2015). Influence of bread
577 structure on human oral processing. *Journal of Food Engineering*, *167*, 147–155.
578 Gibson, L.J.& Ashby, M.F. (1997). Cellular solids, structure and properties.
579 Cambridge Press University, 510 p.
580 Guessasma, S., & Nouri, H. (2015). Comprehensive study of biopolymer foam
581 compression up to densification using X-ray micro-tomography and finite

element computation. *European Polymer Journal*, *72*, 140–148.

Hedjazi, L., Martin, C. L., Guessasma, S., Della Valle, G., & Dendievel, R. (2014). Experimental investigation and discrete simulation of fragmentation in expanded breakfast cereals. *Food Research International*, *55*, 28–36.

Hibberd, G. E., & Parker, N. S. (1985). Measurements of the Compression Properties of Bread Crumb. *Journal of Texture Studies*, *16*(1), 97–110.

Hoebler, C., Devaux, M. F., Karinthi, A., Belleville, C., & Barry, J. L. (2000). Particle size of solid food after human mastication and in vitro simulation of oral breakdown. *International Journal of Food Sciences and Nutrition*, *51*(5), 353–366.

Hoebler, C., Karinthi, A., Devaux, M.-F. F., Guillon, F., Gallant, D. J. G., Bouchet, B., … Barry, J.-L. L. (1998). Physical and chemical transformations of cereal food during oral digestion in human subjects. *The British Journal of Nutrition*, *80*(5), 429–436.

Jalabert-Malbos, M.-L., Mishellany-Dutour, A., Woda, A., & Peyron, M.-A. (2007). Particle size distribution in the food bolus after mastication of natural foods. *Food Quality and Preference*, *18*(5), 803–812.

Jourdren, S., Panouillé, M., Saint-Eve, A., Déléris, I., Forest, D., Lejeune, P., & Souchon, I. (2016). Breakdown pathways during oral processing of different breads: impact of crumb and crust structures. *Food & Function*, *7*(3), 1446–57.

Jourdren, S., Saint-Eve, A., Panouillé, M., Lejeune, P., Déléris, I., & Souchon, I. (2016). Respective impact of bread structure and oral processing on dynamic texture perceptions through statistical multiblock analysis. *Food Research International*, *87*, 142–151.

Kansou, K., Chiron, H., Valle, G. Della, Ndiaye, A., Roussel, P., & Shehzad, A.

(2013). Modelling Wheat Flour Dough Proofing Behaviour: Effects of Mixing Conditions on Porosity and Stability. *Food and Bioprocess Technology*, *6*(8), 2150–2164.

Kim, E. H. J., Corrigan, V. K., Wilson, A. J., Waters, I. R., Hedderley, D. I., & Morgenstern, M. P. (2012). Fundamental fracture properties associated with sensory hardness of brittle solid foods. *Journal of Texture Studies*, *43*(1), 49–62.

Laguna, L., Aktar, T., Ettelaie, R., Holmes, M., & Chen, J. (2016). A Comparison Between Young and Elderly Adults Investigating the Manual and Oral Capabilities During the Eating Process. *Journal of Texture Studies*, *47*(4), 361–372.

Laguna, L., Sarkar, A., Artigas, G., & Chen, J. (2015). A quantitative assessment of the eating capability in the elderly individuals. *Physiology & Behavior*, *147*, 274–281.

Laguna, L., Sarkar, A., & Chen, J. (2015). Assessment of eating capability of elderly subjects in UK: a quantitative evaluation. *Proceedings of the Nutrition Society*, *74*(OCE2), E167.

Lassoued, N., Babin, P., Della Valle, G., Devaux, M. F., & Réguerre, A. L. (2007). Granulometry of bread crumb grain: Contributions of 2D and 3D image analysis at different scale. *Food Research International*, *40*(8), 1087–1097.

Le Bleis, F., Chaunier, L., Della Valle, G., Panouillé, M., & Réguerre, A. L. (2013). Physical assessment of bread destructuration during chewing. *Food Research International*, *50*(1), 308–317.

Le Bleis, F., Chaunier, L., Montigaud, P., & Della Valle, G. (2016). Destructuration mechanisms of bread enriched with fibers during mastication. *Food Research International*, *80*, 1–11.

Lucas, P. W., & Luke, D. A. (1983). Computer simulation of the breakdown of carrot particles during human mastication. *Archives of Oral Biology*, *28*(9), 821–826.

Lucas, P. W., Prinz, J. F., Agrawal, K. R., & Bruce, I. C. (2002). Food physics and oral physiology. *Food Quality and Preference*, *13*(4), 203–213.

Mihai, L. A., & Goriely, A. (2015). Finite deformation effects in cellular structures with hyperelastic cell walls. *International Journal of Solids and Structures*, *53*, 107–128.

Mohammed, M. A. P., Tarleton, E., Charalambides, M. N., & Williams, J. G. (2013). Mechanical characterization and micromechanical modeling of bread dough. *Journal of Rheology*, *57*(1), 249–272.

Olthoff, L. W., Van Der Bilt, A., Bosman, F., & Kleizen, H. H. (1984). Distribution of particle sizes in food comminuted by human mastication. *Archives of Oral Biology*, *29*(11), 899–903.

Panouillé, M., Saint-Eve, A., Déléris, I., Le Bleis, F., & Souchon, I. (2014). Oral processing and bolus properties drive the dynamics of salty and texture perceptions of bread. *Food Research International*, *62*, 238–246.

Panouillé, M., Saint-Eve, A., & Souchon, I. (2016). Instrumental methods for bolus characterization during oral processing to understand food perceptions. *Current Opinion in Food Science*, *9*, 42–49.

Pascua, Y., Koç, H., & Foegeding, E. A. (2013). Food structure: Roles of mechanical properties and oral processing in determining sensory texture of soft materials. *Current Opinion in Colloid & Interface Science*, *18*(4), 324–333.

Peleg, M. (1993). Tailoring texture for the elderly: Theoretical aspects and technological options. *Critical Reviews in Food Science and Nutrition*, *33*(1), 45–55.

Pentikäinen, S., Sozer, N., Närväinen, J., Ylätalo, S., Teppola, P., Jurvelin, J., … Poutanen, K. (2014). Effects of wheat and rye bread structure on mastication process and bolus properties. *Food Research International*, *66*, 356–364.

Peyron, M.-A., Gierczynski, I., Hartmann, C., Loret, C., Dardevet, D., Martin, N., & Woda, A. (2011). Role of Physical Bolus Properties as Sensory Inputs in the Trigger of Swallowing. *PLoS ONE*, *6*(6), e21167.

Peyron, M.-A., Mishellany, A., & Woda, A. (2004). Particle Size Distribution of Food Boluses after Mastication of Six Natural Foods. *Journal of Dental Research*, *83*(7), 578–582.

Peyron, M. A., Woda, A., Bourdiol, P., & Hennequin, M. (2017). Age-related changes in mastication. *Journal of Oral Rehabilitation*, *44*(4), 299–312.

Prinz, J. F., & Lucas, P. W. (1997). An optimization model for mastication and swallowing in mammals. *Proceedings of the Royal Society of London B: Biological Sciences*, *264*(1389).

Rodrigues, S. A., Young, A. K., James, B. J., & Morgenstern, M. P. (2014). Structural changes within a biscuit bolus during mastication. *Journal of Texture Studies*, *45*(2), 89–96.

Scanlon, M. G., & Zghal, M. C. (2001). Bread properties and crumb structure. *Food Research International*, *34*(10), 841–864.

Schwartz, C., Vandenberghe-Descamps, M., Sulmont-Rossé, C., Tournier, C., & Feron, G. (2017). Behavioral and physiological determinants of food choice and consumption at sensitive periods of the life span, a focus on infants and elderly. *Innovative Food Science & Emerging Technologies*.

Serra, J. P. (1982). *Image analysis and mathematical morphology*. Academic Press. Retrieved from https://books.google.co.uk/books?id=6pZTAAAAYAAJ

682 Ship, J. A. (1999). The Influence of Aging on Oral Health and Consequences for
683 Taste and Smell. *Physiology & Behavior*, *66*(2), 209–215.
684 Sozer, N., Dogan, H., & Kokini, J. L. (2011). Textural properties and their correlation
685 to cell structure in porous food materials. *Journal of Agricultural and Food*
686 *Chemistry*, *59*(5), 1498–1507.
687 United Nations Department of Economic and Social Affairs. (2002). World population
688 ageing, 1950-2050. Retrieved July 27, 2017, from
689 http://www.un.org/esa/population/publications/worldageing19502050/
690 van der Bilt, A., Olthoff, L. W., van der Glas, H. W., van der Weelen, K., & Bosman,
691 F. (1987). A mathematical description of the comminution of food in human
692 mastication. *Archives of Oral Biology*, *32*(8), 579–588.
693 van der Glas, H. W., Kim, E. H. J., Mustapa, A. Z., & Elmanaseer, W. R. (2018).
694 Selection in mixtures of food particles during oral processing in man. *Archives of*
695 *Oral Biology*, *85*(August 2017), 212–225.
696 van der Glas, H. W., van der Bilt, A., & Bosman, F. (1992). A selection model to
697 estimate the interaction between food particles and the post-canine teeth in
698 human mastication. *Journal of Theoretical Biology*, *155*(1), 103–120.
699 Van Dyck, T., Verboven, P., Herremans, E., Defraeye, T., Van Campenhout, L.,
700 Wevers, M., … Nicolaï, B. (2014). Characterisation of structural patterns in bread
701 as evaluated by X-ray computer tomography. *Journal of Food Engineering*, *123*,
702 67–77.
703 Vandenberghe-Descamps, M., Labouré, H., Prot, A., Septier, C., Tournier, C., Feron,
704 G., & Sulmont-Rossé, C. (2016). Salivary Flow Decreases in Healthy Elderly
705 People Independently of Dental Status and Drug Intake. *Journal of Texture*
706 *Studies*, *47*(4), 353–360.

Wang, S., Austin, P., & Bell, S. (2011). It's a maze: The pore structure of bread crumbs. *Journal of Cereal Science*, *54*(2), 203–210.

Witt, T., & Stokes, J. R. (2015). Physics of food structure breakdown and bolus formation during oral processing of hard and soft solids. *Current Opinion in Food Science*, *3*, 110–117.

Young, A. K., Cheong, J. N., Hedderley, D. I., Morgenstern, M. P., & James, B. J. (2013). Understanding the link between bolus properties and perceived texture. *Journal of Texture Studies*, *44*(5), 376–386.

Yven, C., Guessasma, S., Chaunier, L., Della Valle, G., & Salles, C. (2010). The role of mechanical properties of brittle airy foods on the masticatory performance. *Journal of Food Engineering*, *101*(1), 85–91.

720 **List of Figures**

721 Fig.1: (a) Crumb cross-sections and (b) 2D (top) , 3D (bottom) images of sponge
722 cake and brioche (diameter = 20mm) obtained by micro-computed tomography (XR-
723 µCT) and (c) the resulting cumulated size distribution of walls (dotted line) and cells
724 (continuous line) for sponge-cake (blue) and brioche (red).

725 Fig.2: Average stress-strain curves obtained by uniaxial compression of the two
726 cereal foods: sponge-cake (blue) and brioche (red). Error bars reflect the standard
727 deviation obtained from 5 replicates.

728 Fig.3: Examples of cumulative size distribution curves of bolus particles for the three
729 chewing time values C1 (blue), C2 (red) and SP (green), and their corresponding
730 fitting by Gompertz model (dotted lines), for sponge cake (a) and, in the case of
731 brioche, for the three patterns of fragmentation / agglomeration, I, II and III
732 respectively (b, c, d).

733 Fig.4: Variations of median particle size (D_{50}) and interquartile ratio (D_{75}/D_{25}) with
734 chewing time for sponge-cake (a, blue) and brioche (b, red). Empty symbols:
735 satisfactory dental status, filled symbols: poor dental status.

736 Fig. 5: Variations of c and b values derived from Gompertz model with respectively
737 (a) particle median size (D_{50}) and (b) interquartile ratio (D_{75}/D_{25}) for sponge cake
738 (blue) and brioche (red).

739 Fig.6: Typical examples of boli images after chewing at C1 (left), C2 (center) and at
740 swallowing point (right) for sponge-cake (a), and for brioche, decreasing size (case I)
741 (b), increasing size (case II) (c), combination of both (case III) (d). These images
742 correspond to the size distributions plotted in Fig.3.

743

744

745 **List of Tables**

749

List of Tables

List of Figures

(a)

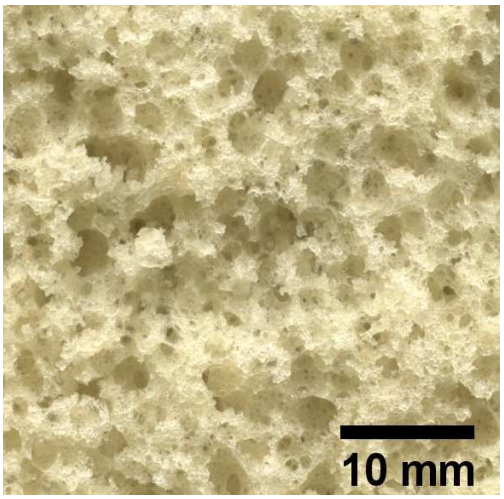

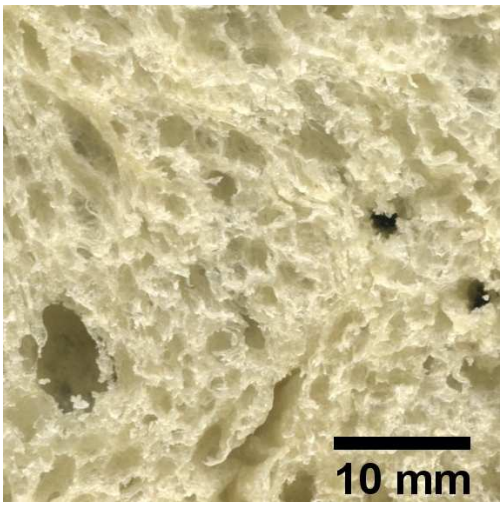

(b)

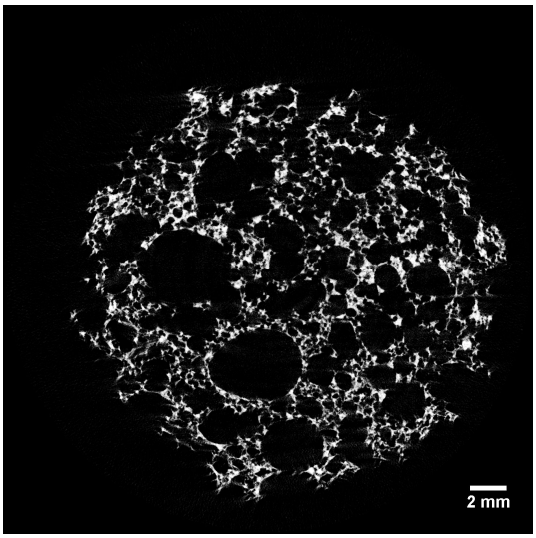

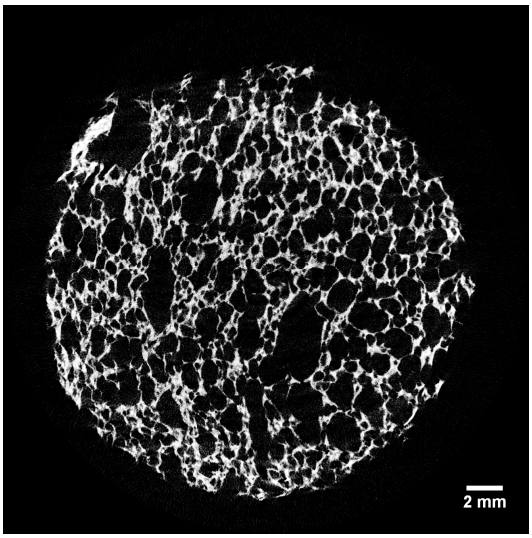

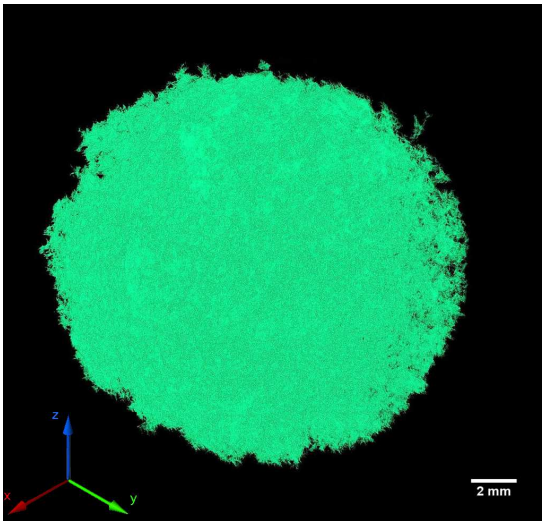

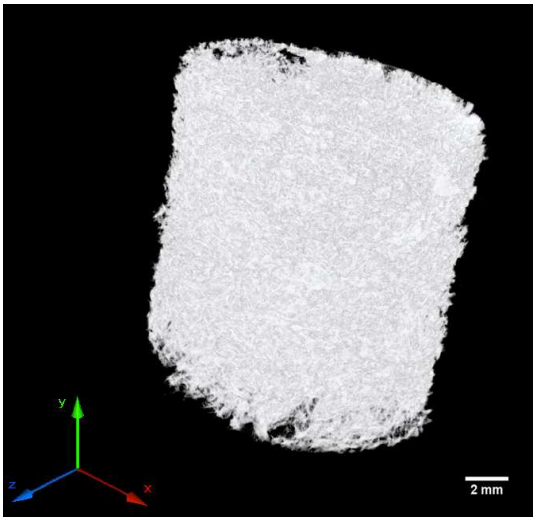

c)

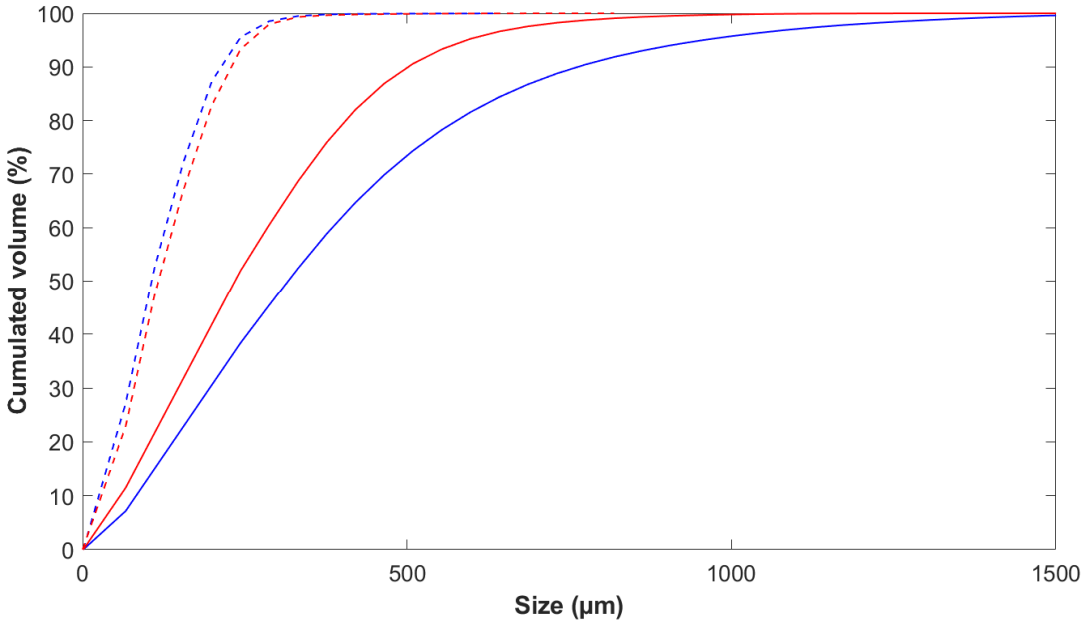

Fig1. Fragmentation soft cereals Assad-Bustillos et al.

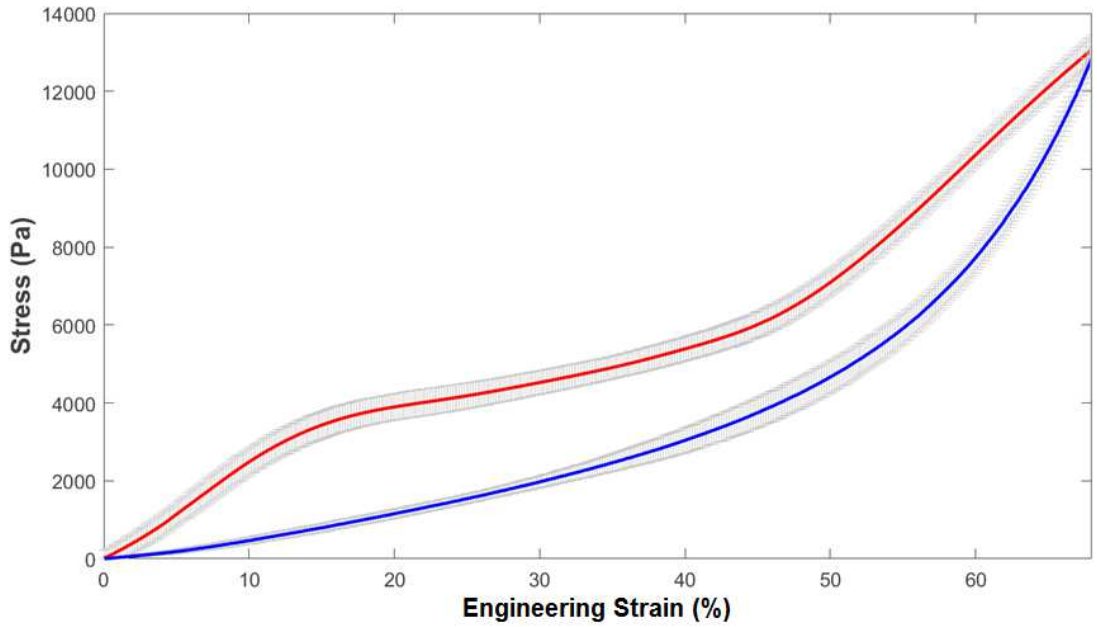

Fig.2 Fragmentation soft cereals Assad-Bustillos et al.

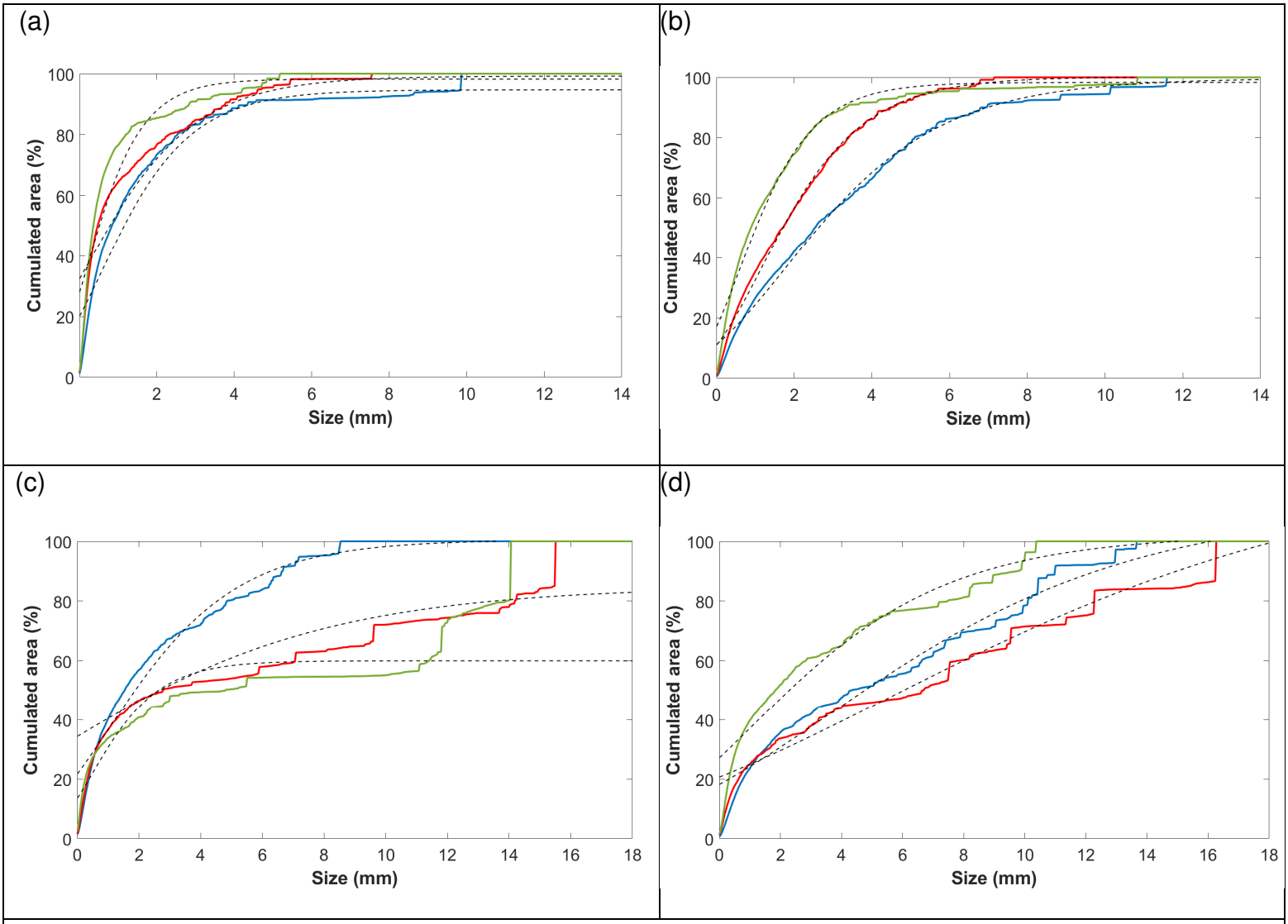

Fig.3 Fragmentation soft cereals Assad-Bustillos et al.

(a)

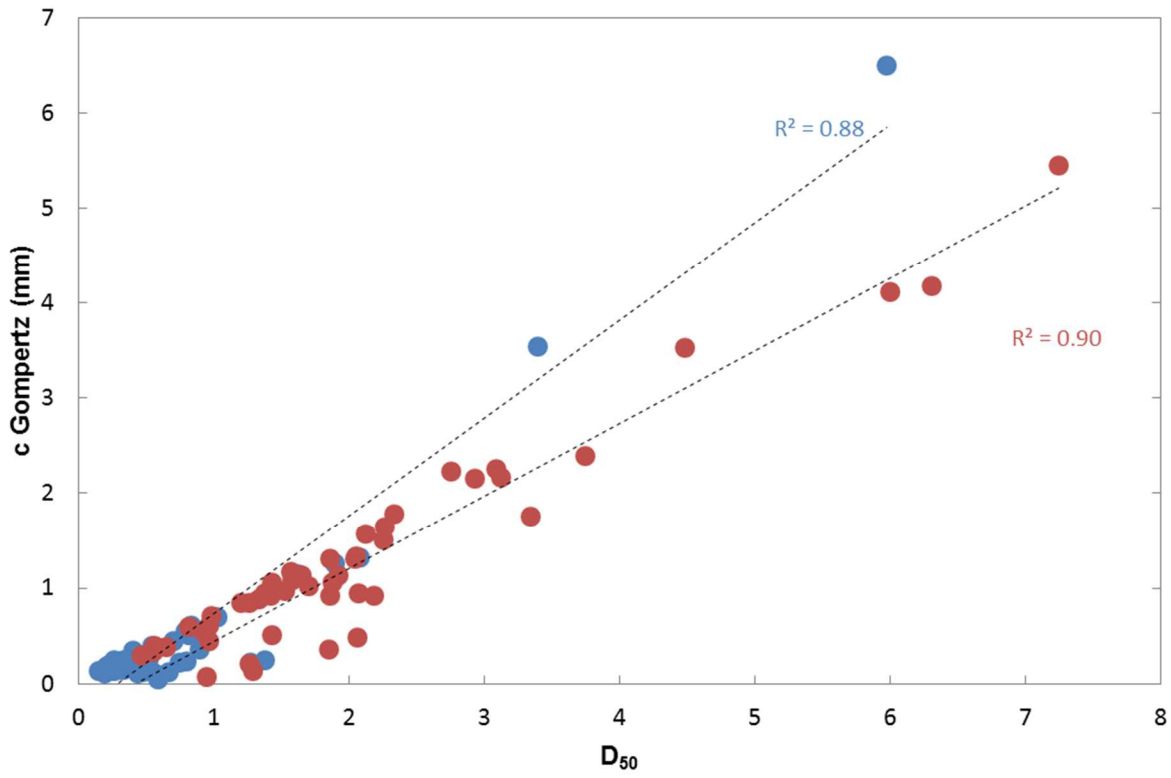

(b)

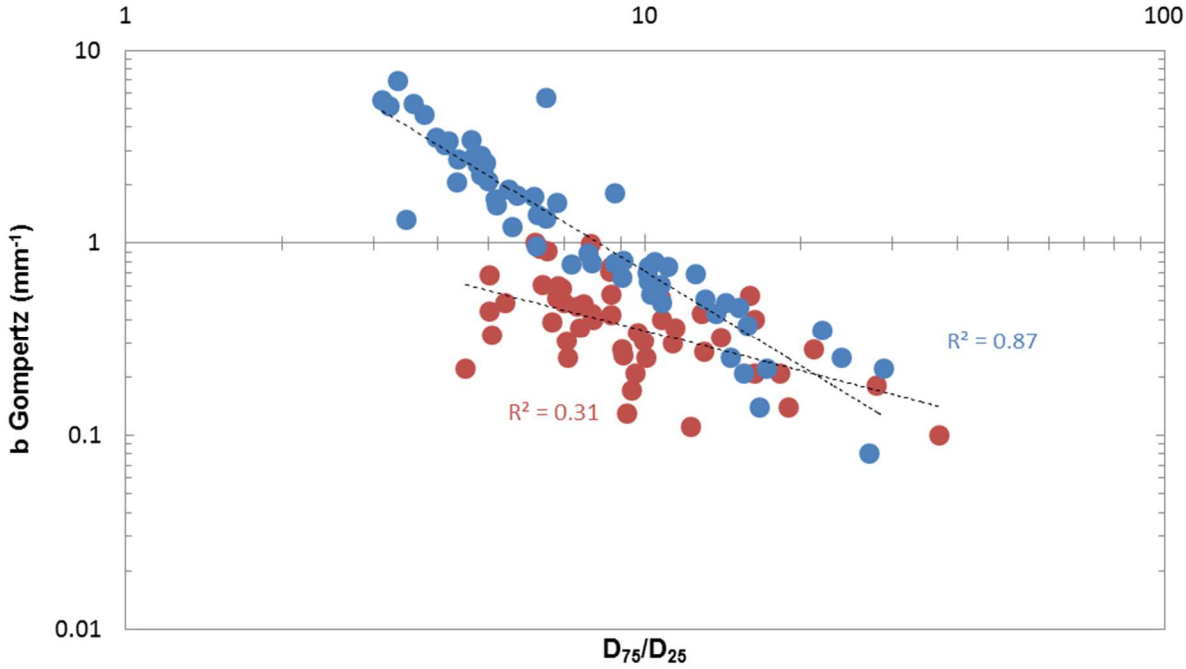

Fig.5 Fragmentation soft cereals Assad-Bustillos et al.

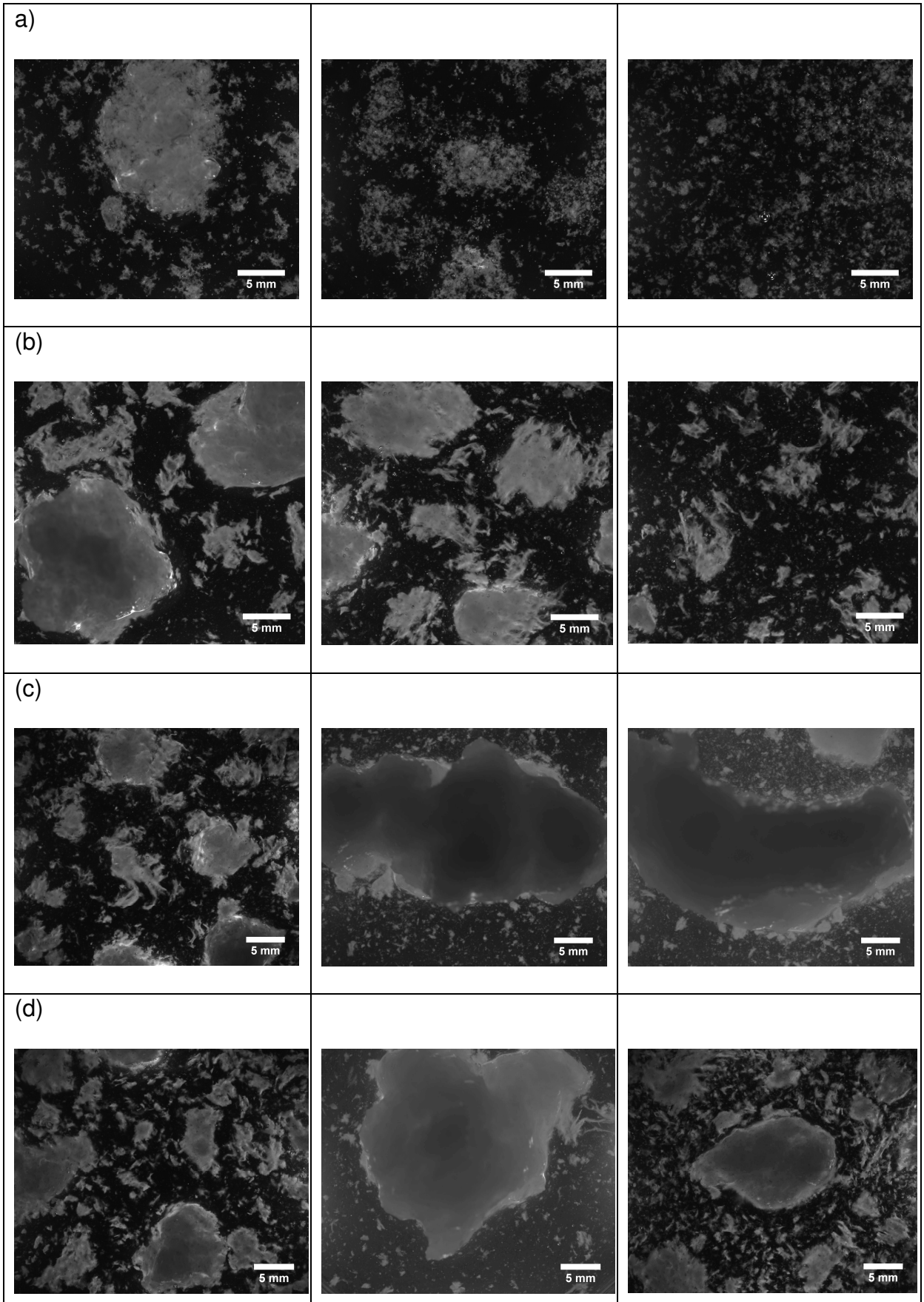

Fig.6 Fragmentation soft cereals Assad-Bustillos et al.

	Sponge-cake	Brioche
Direct Measures*		
Density (g/cm^3)	0.21 (±0.02)^A	0.33 (±0.02)^B
Young's modulus E (kPa)	5 (±1)^A	20 (±3)^B
Critical stress σ_c (kPa)	N/A	3 (±1)
3D Image Analysis**		
Porosity	0.79 (±0.01)^B	0.69 (±0.04)^A
Relative density (D)	0.21 (±0.01)^A	0.31 (±0.04)^B
Wall Size		
D_{25}	41 (±1)^A	45 (±1)^B
D_{50}	99 (±1)^A	118 (±5)^A
D_{75}	176 (±1)^A	200 (±12)^A
Cell size		
D_{25}	95 (±1)^B	73 (±10)^A
D_{50}	296 (±2)^B	197 (±26)^A
D_{75}	785 (±81)^B	403 (±40)^A

**Values are average of n=5 measures (±Std. deviation).*
*** Values are average of n=2 measures (±Std. deviation).*
Different letters (A, B), indicate means that significantly ($p<0.05$) differ between products (Student-Newman-Keuls test).

Table 2. Fragmentation soft cereals Assad-Bustillos et al.

Product	Parameter	Chewing sequence		
		C1	*C2*	*SP*
Sponge-cake	D_{50}	1.1 (±1.3)$^{a\,A}$	0.5 (±0.7)$^{b\,A}$	0.3 (±0.1)$^{c\,A}$
	D_{75}/D_{25}	13.3 (±6.1)$^{a\,A}$	8.9 (±5.7)$^{b\,A}$	5.0 (±2.1)$^{c\,A}$
	a	100.8 (±12.6)$^{a\,A}$	100.4 (±7.6)$^{a\,A}$	99.3 (±0.5)$^{a\,A}$
	b	0.7 (±0.5)$^{a\,A}$	1.4 (±1.2)$^{b\,A}$	2.7 (±1.6)$^{c\,A}$
	c	0.7 (±1.5)$^{a\,A}$	0.3 (±0.9)$^{b\,A}$	0.2 (±0.1)$^{c\,A}$
Brioche	D_{50}	2.5 (±1.5)$^{a\,B}$	2.5 (±2.3)$^{a\,B}$	2.9 (±4.0)$^{a\,B}$
	D_{75}/D_{25}	8.3 (±3.4)$^{a\,B}$	15.2 (±14.4)$^{a\,B}$	25.6 (±24.2)$^{b\,B}$
	a	108.7 (±39.4)$^{a\,A}$	106.7 (±28.3)$^{a\,A}$	102.2 (±10.1)$^{a\,A}$
	b	0.4 (±0.1)$^{a\,B}$	0.4 (±0.2)$^{a\,B}$	0.5 (±0.3)$^{a\,B}$
	c	2.4 (±3.7)$^{a\,B}$	1.9 (±3.0)$^{a\,B}$	-0.3 (±3.4)$^{b\,A}$

Note: All values are means (±Std. deviation) of n=20 subjects. The negative mean value of c for brioche bolus at SP means that many small particles have a size value below image resolution.
Different letters (a,b,c) indicate means that significantly ($p<0.05$) differ between chewing sequences (Student-Newman-Keuls test).
Different letters (A, B), indicate means that significantly ($p<0.05$) differ between products (Student-Newman-Keuls test).

(a)

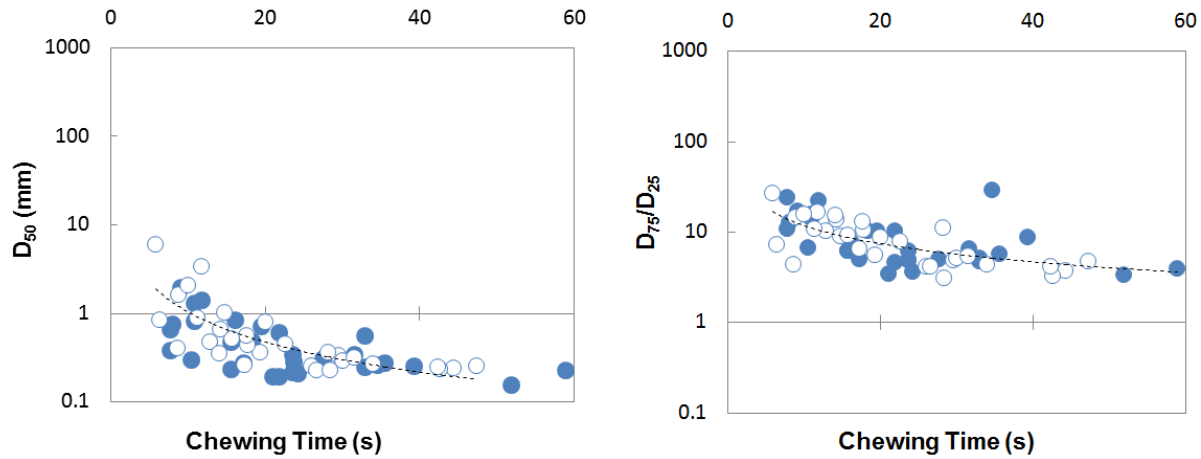

(b)

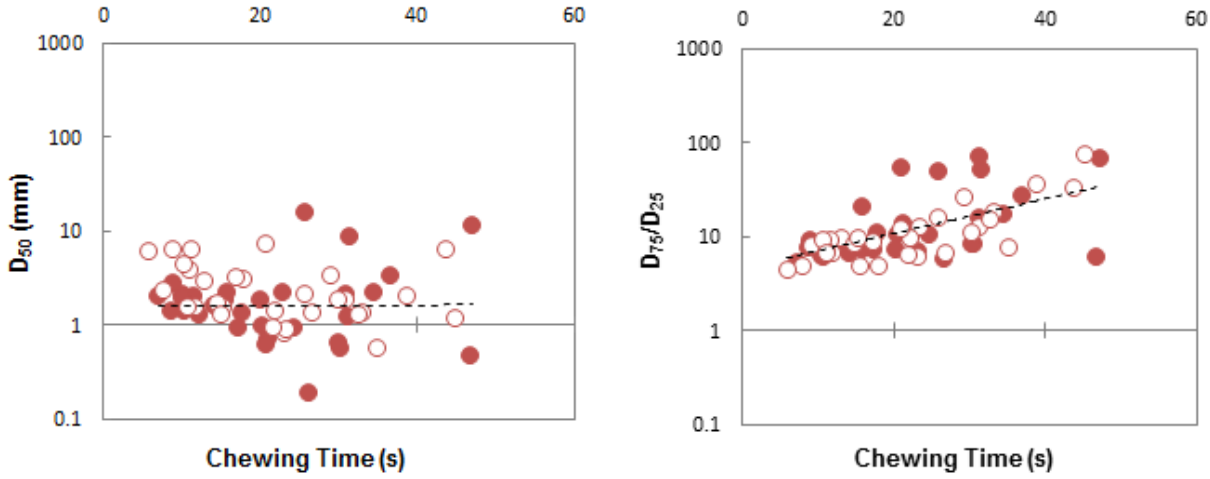

Fig.4 Fragmentation soft cereals Assad-Bustillos et al.

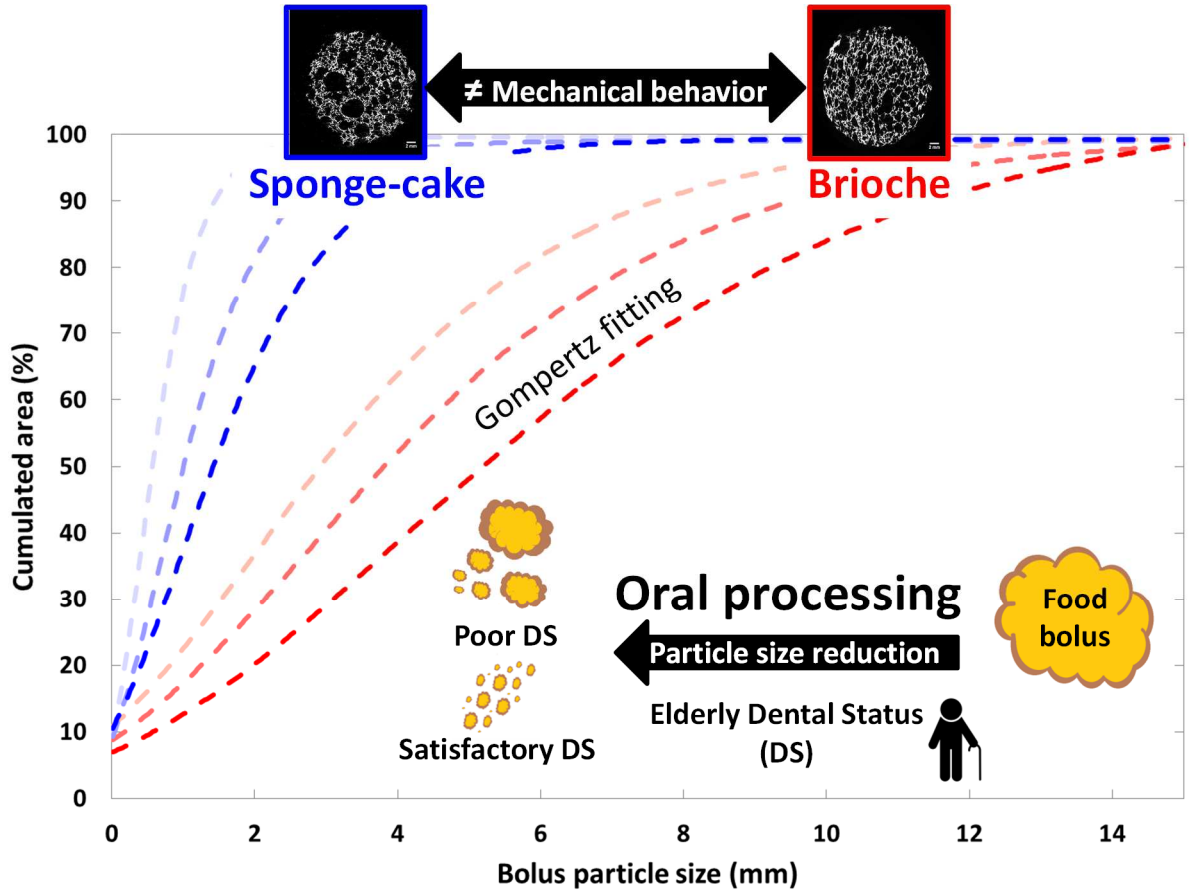

Graphical Abstract for "Cereal FOP fragmentation" by Assad-Bustillos et al.:

The mechanisms of fragmentation of soft cereal foods during chewing are determined by image analysis and by fitting particle size distributions. This approach has allowed us to link food structure and mechanical behavior on one side, with the dental status of elderly on the other side.